



International Journal of Innovative Research in Science Engineering and Technology (IJIRSET)

(A Monthly, Peer Reviewed, Refereed, Scholarly Indexed, Open Access Journal)



Impact Factor: 9.935

Volume 15, Issue 6, June 2026

Spectral, Transmittance and Thermal Properties of Pr³⁺ Doped Bismuth Borate Glasses with Large Fluorescence Life Time

S.L.Meena

Ceramic Laboratory, Department of Physics, Jai Narain Vyas University, Jodhpur, Rajasthan, India

ABSTRACT: Zinc lithium alumino tungsten lead bismuth borate glasses containing Pr³⁺ in (35-x):Bi₂O₃:10ZnO:10Li₂O:10Al₂O₃:10WO₃:10PbO:15B₂O₃:xPr₂O₃ (where x=1, 1.5,2 mol %) have been prepared by melt-quenching method. The amorphous nature of the glasses was confirmed by x-ray diffraction studies. DTA curve was analysed to evaluate the glass transition temperature, crystallization temperature and melting temperature. Optical absorption, Excitation spectra and fluorescence spectra were recorded at room temperature for all glass samples. Judd-Ofelt intensity parameters Ω_λ ($\lambda=2, 4, 6$) are evaluated from the intensities of various absorption bands of optical absorption spectra. Using these intensity parameters various radiative properties like spontaneous emission probability, branching ratio, radiative life time and stimulated emission cross-section of various emission lines have been evaluated.

KEYWORDS: ZLATLBB Glasses, Optical Properties, Judd-Ofelt Theory, Thermal Properties.

I. INTRODUCTION

Transparent glass-ceramic have attracted great interest due to their potential application in optical devices such as optical fiber amplifiers, lasers and frequency-conversion materials, [1–5]. Borate glasses have wide range applications in the field of glass ceramics such as low phonon energy, large transparency window, good thermal stability, high refractive index, good mechanical, high density and chemical durability [6-10]. Borate glasses are very important because of the possibility of their application in optoelectronic, optic device fields, lasers, fiber optic large bandwidth and solar cells [11-13]. The addition of network modifier (NWF) Li₂O is to improve both mechanical and electrical properties of such glasses. Recently, rare earth doped borate glass has attracted much interest because of high rare earth ion solubility, optical data transmission, detection, sensor and catalysts [14-16].

In this work, the spectroscopic properties of Pr³⁺ -doped (35-x):Bi₂O₃:10ZnO:10Li₂O:10Al₂O₃:10WO₃:10PbO:15B₂O₃:xPr₂O₃ (where x=1, 1.5,2 mol %) glasses were investigated. absorption, Excitation spectra and fluorescence spectra, The absorption, Excitation and fluorescence spectra of Pr³⁺ of the glasses were investigated. The J-O intensity parameters render significant information regarding local structure and bonding in the vicinity of rare- earth ions.

II. EXPERIMENTAL TECHNIQUES

Preparation of glasses

The following Pr³⁺ doped zinc lithium alumino tungsten lead bismuth borate glass samples (35-x): Bi₂O₃: 10ZnO: 10Li₂O: 10Al₂O₃: 10WO₃: 10PbO: 15B₂O₃: xPr₂O₃ (where x=1, 1.5,2) have been prepared by melt-quenching method. Analytical reagent grade chemical used in the present study consist of Bi₂O₃, ZnO, Li₂O, Al₂O₃, WO₃, PbO, B₂O₃ and Pr₂O₃. All weighed chemicals were powdered by using an Agate pestle mortar and mixed thoroughly before each batch (10g) was melted in alumina crucibles in silicon carbide based an electrical furnace.

Silicon Carbide Muffle furnace was heated to working temperature of 980⁰C, for preparation of zinc lithium alumino tungsten lead bismuth borate glasses, for two hours to ensure the melt to be free from gases. The melt was stirred several times to ensure homogeneity. For quenching, the melt was quickly poured on the steel plate & was immediately inserted in the muffle furnace for annealing. The steel plate was preheated to 100⁰C. While pouring; the temperature of crucible was also maintained to prevent crystallization. And annealed at temperature of 350⁰C for 2h to remove thermal

strains and stresses. Every time fine powder of cerium oxide was used for polishing the samples. The glass samples so prepared were of good optical quality and were transparent. The chemical compositions of the glasses with the name of samples are summarized in Table 1

Table 1 Chemical composition of the glasses

Sample	Glass composition (mol %)
ZLATLBB (UD)	35Bi ₂ O ₃ :10ZnO:10Li ₂ O:10Al ₂ O ₃ :10WO ₃ :10PbO:15B ₂ O ₃
ZLATLBB PR (1.0)	34Bi ₂ O ₃ :10ZnO:10Li ₂ O:10Al ₂ O ₃ :10WO ₃ :10PbO:15B ₂ O ₃ :1 Pr ₂ O ₃
ZLATLBB PR (1.5)	33.5Bi ₂ O ₃ :10ZnO:10Li ₂ O:10Al ₂ O ₃ :10WO ₃ :10PbO:15B ₂ O ₃ : 1.5 Pr ₂ O ₃
ZLATLBB PR (2.0)	33Bi ₂ O ₃ :10ZnO:10Li ₂ O:10Al ₂ O ₃ :10WO ₃ :10PbO:15B ₂ O ₃ : 2 Pr ₂ O ₃

ZLATLBB (UD)—Represents undoped Zinc Lithium Alumino Tungsten Lead Bismuth Borate glass specimen.
ZLATLBB (PR) -Represents Pr³⁺ Zinc Lithium Alumino Tungsten Lead Bismuth Borate glass specimens.

III. THEORY

3.1 Oscillator Strength

The intensity of spectral lines are expressed in terms of oscillator strengths using the relation [17].

$$f_{\text{expt.}} = 4.318 \times 10^{-9} \int \epsilon(\nu) d\nu \quad (1)$$

where, $\epsilon(\nu)$ is molar absorption coefficient at a given energy ν (cm⁻¹), to be evaluated from Beer–Lambert law.

Under Gaussian Approximation, using Beer–Lambert law, the observed oscillator strengths of the absorption bands have been experimentally calculated, using the modified relation [18].

$$P_m = 4.6 \times 10^{-9} \times \frac{1}{cl} \log \frac{I_0}{I} \times \Delta\nu_{1/2} \quad (2)$$

where c is the molar concentration of the absorbing ion per unit volume, l is the optical path length, $\log I_0/I$ is absorbivity or optical density and $\Delta\nu_{1/2}$ is half band width.

3.2 Judd-Ofelt Intensity Parameters

According to Judd [19] and Ofelt [20] theory, independently derived expression for the oscillator strength of the induced forced electric dipole transitions between an initial J manifold $|4f^N(S, L) J\rangle$ level and the terminal J' manifold $|4f^N(S', L') J'\rangle$ is given by:

$$\frac{8\pi^2 m c \nu}{3h(2J+1)n} \frac{1}{n} \left[\frac{(n^2+2)^2}{9} \right] \times S(J, J') \quad (3)$$

where, the line strength $S(J, J')$ is given by the equation

$$S(J, J') = e^2 \sum_{\lambda=2, 4, 6} \Omega_{\lambda} \langle 4f^N(S, L) J || U^{(\lambda)} || 4f^N(S', L') J' \rangle^2 \quad (4)$$

In the above equation m is the mass of an electron, c is the velocity of light, ν is the wave number of the transition, h is Planck's constant, n is the refractive index, J and J' are the total angular momentum of the initial and final level respectively, Ω_{λ} ($\lambda = 2, 4$ and 6) are known as Judd-Ofelt intensity parameters.

3.3. Radiative Properties

The Ω_λ parameters obtained using the absorption spectral results have been used to predict radiative properties such as spontaneous emission probability (A) and radiative life time (τ_R), and laser parameters like fluorescence branching ratio (β_R) and stimulated emission cross section (σ_p).

The spontaneous emission probability from initial manifold $|4f^N(S', L') J' \rangle$ to a final manifold $|4f^N(S, L) J \rangle$ is given by:

$$A[(S', L') J'; (S, L) J] = \frac{64 \pi^2 \nu^3}{3h(2J'+1)} \left[\frac{n(n^2+2)^2}{9} \right] \times S(J', \bar{J}) \quad (5)$$

Where, $S(J', J) = e^2 [\Omega_2 \|U^{(2)}\|^2 + \Omega_4 \|U^{(4)}\|^2 + \Omega_6 \|U^{(6)}\|^2]$

The fluorescence branching ratio for the transitions originating from a specific initial manifold $|4f^N(S', L') J' \rangle$ to a final manifold $|4f^N(S, L) J \rangle$ is given by

$$\beta[(S', L') J'; (S, L) J] = \sum_{S L J} \frac{A[(S', L') J'; (S, L) J]}{A[(S', L') J'; (S, L) J]} \quad (6)$$

where, the sum is over all terminal manifolds.

The radiative life time is given by

$$\tau_{rad} = \sum_{S L J} A[(S', L') J'; (S, L) J] = A_{Total}^{-1} \quad (7)$$

where, the sum is over all possible terminal manifolds. The stimulated emission cross-section for a transition from an initial manifold $|4f^N(S', L') J' \rangle$ to a final manifold $|4f^N(S, L) J \rangle$ is expressed as

$$\sigma_p(\lambda_p) = \left[\frac{\lambda_p^4}{8\pi c n^2 \Delta\lambda_{eff}} \right] \times A[(S', L') J'; (S, L) J] \quad (8)$$

where, λ_p the peak fluorescence wavelength of the emission band and $\Delta\lambda_{eff}$ is the effective fluorescence line width.

3.4 Nephelauxetic Ratio (β) and Bonding Parameter ($b^{1/2}$)

The nature of the R-O bond is known by the Nephelauxetic Ratio (β') and Bonding Parameters ($b^{1/2}$), which are computed by using following formulae [21, 22]. The Nephelauxetic Ratio is given by

$$\beta' = \frac{\nu_g}{\nu_a} \quad (9)$$

where, ν_a and ν_g refer to the energies of the corresponding transition in the glass and free ion, respectively. The values of bonding parameter $b^{1/2}$ are given by

$$b^{1/2} = \left[\frac{1-\beta'}{2} \right]^{1/2} \quad (10)$$

IV. RESULT AND DISCUSSION

4.1. XRD Measurement

Figure 1 presents the XRD pattern of the samples containing show no sharp Bragg's peak, but only a broad diffuse hump around low angle region. This is the clear indication of amorphous nature with in the resolution limit of XRD instrument.

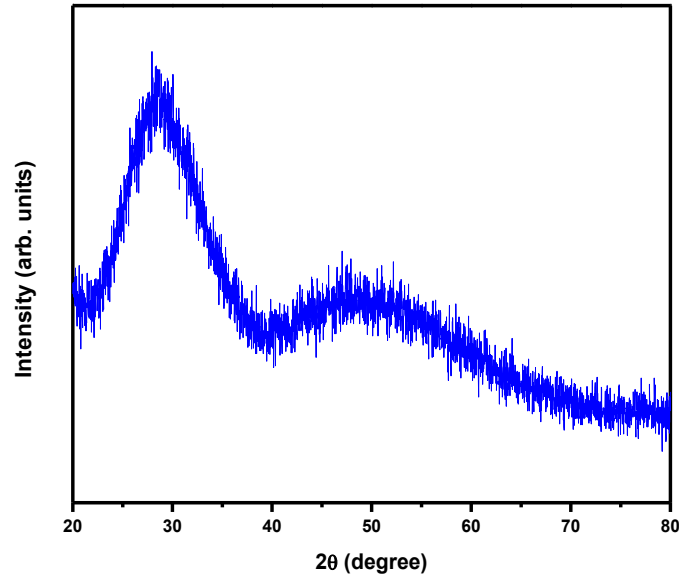


Fig.1: X-ray diffraction pattern of ZLATLBB PR(1.0) glass.

4.2 Transmittance Spectra

The Transmittance spectrum of ZLATLBB PR(1.0) glass is shown in Figure 2.

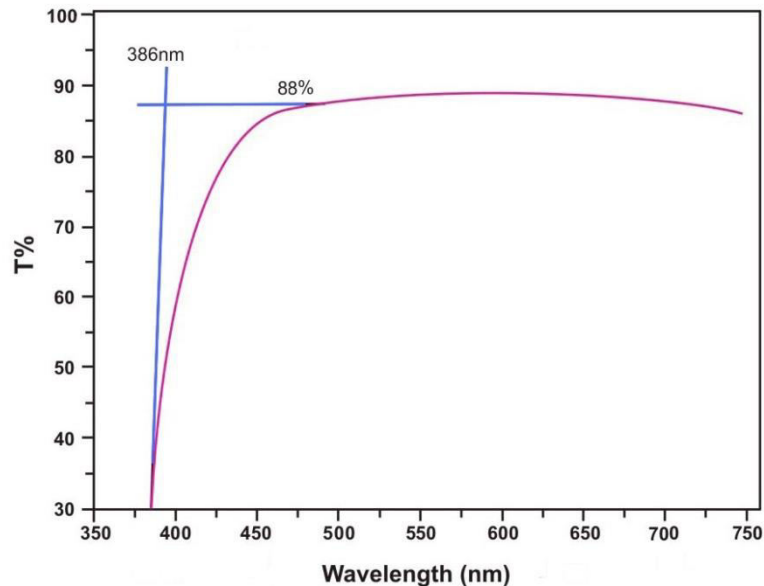


Fig. 2: Transmittance spectrum of ZLATLBB PR(1.0) glass.

4.3 Thermal Property

Differential thermal analysis checks the heat absorbed by glass samples during heating or cooling. Fig. 3 depicts the DTA thermogram of powdered ZLATLBB PR(1.0) sample. The glass transition temperature (T_g), onset crystallization temperature (T_c), crystallization temperature (T_p), melting temperature (T_m), thermal stability (T_s), Balaji Parameter (B_p),

Hurbe’s criterion (H_R) and reduced glass transition temperature (T_{rg}) were calculated. Shankar’s parameter also calculated by using eq. (15). All the determined thermal parameters are given in table 2.

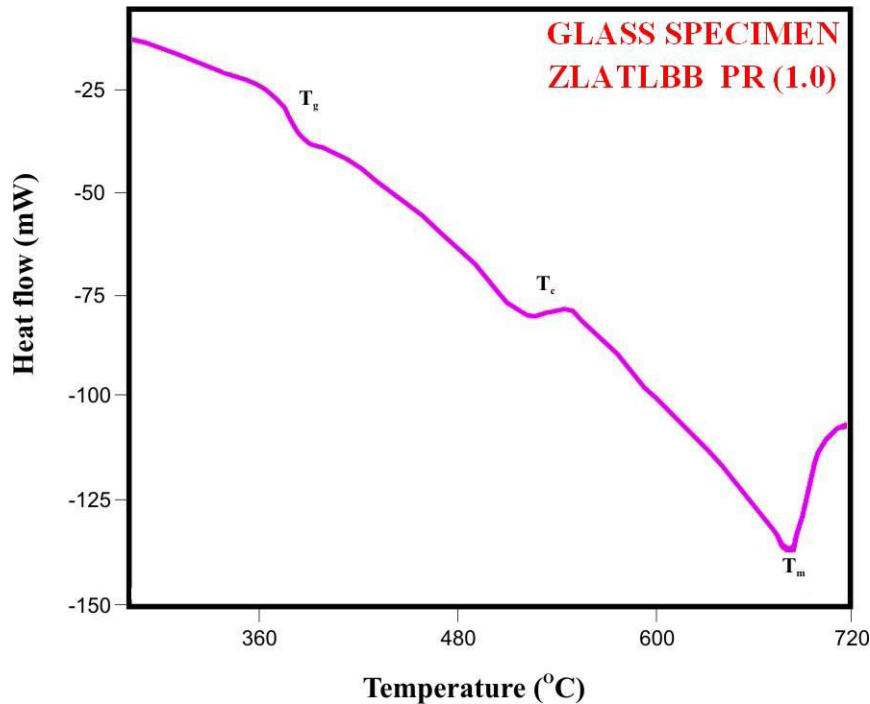


Fig.3: DTA curve of ZLATLBB PR (1.0) glass.

Table2. Thermal parameters determined from the DTA traces of ZLATLBB PR glasses.

Sample Name	T_g (°C)	T_c (°C)	T_p (°C)	T_m (°C)	T_s (°C)	B_p (°C)	H_R (°C)	K_s (°C)	T_{rg} (°C)
ZLATLBB PR (1.0)	375	509	548	685	134	3.436	0.222	34.429	0.547
ZLATLBB PR (1.5)	380	512	550	688	132	3.474	0.216	33.767	0.552
ZLATLBB PR (2.0)	384	513	556	694	129	3.000	0.238	33.644	0.553

The thermal stability of the glass samples can be calculated by difference between onset crystallization temperature and transition temperature [23].

$$\text{Thermal stability } (T_s) = T_c - T_g \quad (11)$$

Balaji Parameter can be calculated using [23].

$$\text{Balaji Parameter } (B_p) = [(T_c - T_g) / (T_p - T_c)] \quad (12)$$

Hruby’s criterion is calculated using the Hurby’s relation [23].

$$\text{Hruby’s criterion } (H_R) = [(T_p - T_c) / (T_m - T_c)] \quad (13)$$

Reduced glass transition temperature is given as [23].

$$\text{Reduced glass transition temperature } (T_{rg}) = T_g \quad (14)$$

Thermal Parameter is given as [23].

$$K_S = [(T_m - T_c)(T_c - T_g) / T_m] \quad (15)$$

4.4 Absorption spectra

The absorption spectra of ZLATLBB PR (1.0) glass, consists of absorption bands corresponding to the absorptions from the ground state 3H_4 of Pr^{3+} ions. Eight absorption bands have been observed from the ground state 3H_4 to excited states 3F_2 , 3F_3 , 3F_4 , 1G_4 , 1D_2 , 3P_0 , 3P_1 and 3P_2 for Pr^{3+} doped ZLATLBB PR(1.0) glass.

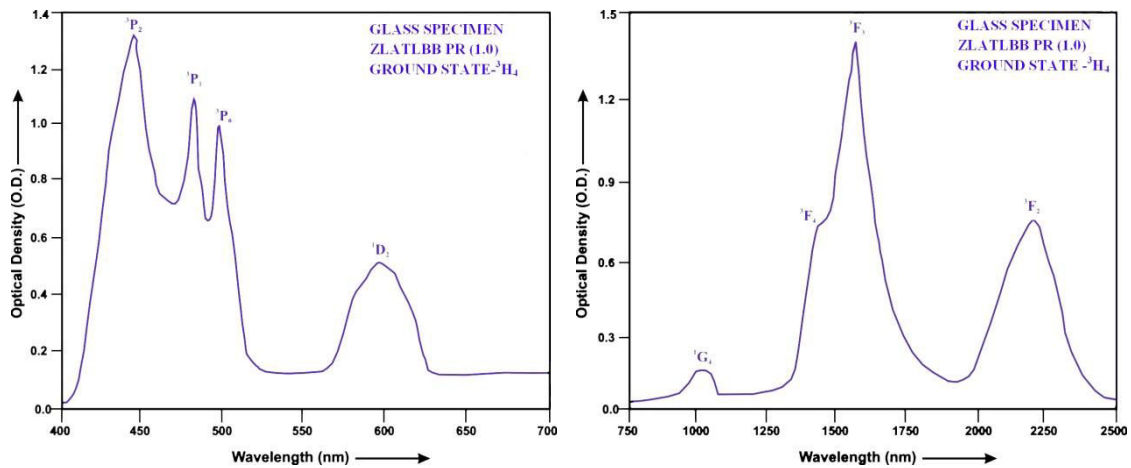


Fig.4: Absorption spectra of ZLATLBB PR (1.0) glass.

The experimental and calculated oscillator strengths for Pr^{3+} ions in zinc lithium alumin tungsten lead bismuth borate glasses are given in Table 3

Table3 Measured and calculated oscillator strength ($P^m \times 10^{+6}$) of Pr^{3+} ions in ZLATLBB glasses.

Energy level 3H_4	Glass ZLATLBB PR(1.0)		Glass ZLATLBB PR(1.5)		Glass ZLATLBB PR(2.0)	
	$P_{exp.}$	$P_{cal.}$	$P_{exp.}$	$P_{cal.}$	$P_{exp.}$	$P_{cal.}$
3F_2	4.66	3.96	3.65	2.97	2.55	2.06
3F_3	6.99	6.11	5.48	4.66	4.74	3.98
3F_4	4.24	3.75	3.54	3.01	2.43	2.49
1G_4	0.35	0.32	0.29	0.25	0.23	0.21
1D_2	2.36	1.08	1.94	0.84	1.36	0.71
3P_0	4.70	1.66	3.68	0.86	2.58	1.02
3P_1	4.83	2.84	3.88	1.66	2.74	1.75
3P_2	12.56	3.57	11.48	2.79	10.56	2.37
R.m.s.deviation	3.4852		3.3717		2.9947	

Computed values of Slater-Condon, Lande', Racah, nephelauxetic ratio and bonding parameter for Pr^{3+} doped ZLATLBB glass specimens are given in Table 4.

Table4. Computed values of Slater-Condon, Lande', Racah, nephelauxetic ratio and bonding parameter for Pr³⁺ doped ZLATLBB glass specimens

Parameter	Free ion	ZLATLBB PR(1.0)	ZLATLBB PR(1.5)	ZLATLBB PR(2.0)
F ₂ (cm ⁻¹)	322.09	300.01	299.99	300.01
F ₄ (cm ⁻¹)	44.46	44.27	44.26	44.27
F ₆ (cm ⁻¹)	4.867	4.412	4.412	4.412
ξ _{4f} (cm ⁻¹)	741.00	858.41	858.59	858.41
E ¹ (cm ⁻¹)	4728.92	4450.98	4450.62	4450.98
E ² (cm ⁻¹)	24.75	22.01	22.01	22.01
E ³ (cm ⁻¹)	478.10	454.74	454.69	454.74
F ₄ /F ₂	0.13804	0.14755	0.14753	0.14755
F ₆ /F ₂	0.01511	0.01470	0.01471	0.01470
E ¹ /E ³	9.8911	9.7881	9.7882	9.7881
E ² /E ³	0.0518	0.0484	0.0484	0.0484
β'		0.8887	0.8886	0.8887
b ^{1/2}		0.2359	0.2360	0.2359

The values of Judd-Ofelt intensity parameters are given in Table 5.

Table5. Judd-Ofelt intensity parameters for Pr³⁺ doped ZLATLBB glass specimens.

Glass Specimen	Ω ₂ (pm ²)	Ω ₄ (pm ²)	Ω ₆ (pm ²)	Ω ₄ /Ω ₆	Ref.
ZLATLBB PR(1.0)	2.820	2.345	5.287	0.4435	P.W.
ZLATLBB PR(1.5)	2.333	1.216	4.299	0.2829	P.W.
ZLATLBB PR(2.0)	1.249	1.435	3.537	0.4057	P.W.
ZTFB (PR)	4.620	3.275	8.632	0.3794	[24].
TWPL (PR)	2.087	1.591	3.780	0.4209	[25].

4.5 Excitation Spectrum

Excitation spectra of ZLATLBB PR (1.0) glass recorded at the emission wavelength 395 nm is depicted as figure 5. The excitation spectra consists of three peaks corresponding to the transitions from the ground state ³H₄ to the various excited states ³P₂, ³P₁ and ³P₀ at the wavelengths of 448, 465 and 486 nm respectively. Among these, a prominent excitation band at 448 nm has been selected for the measurement of emission spectrum of Pr³⁺ glass.

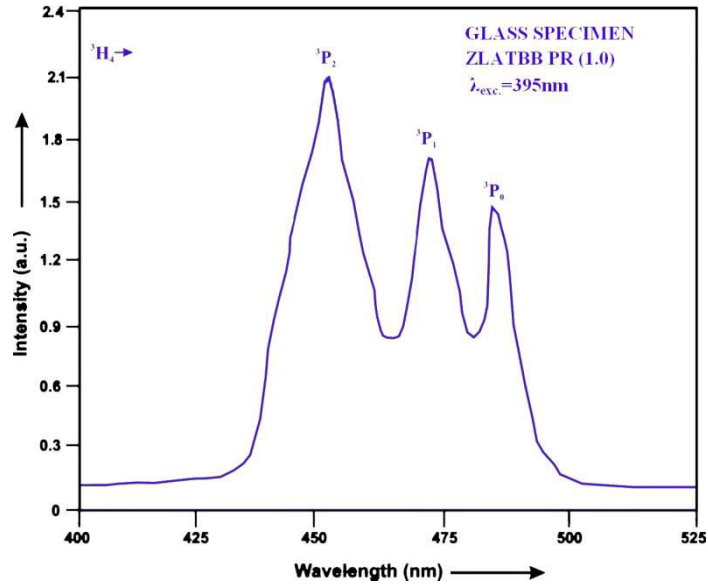
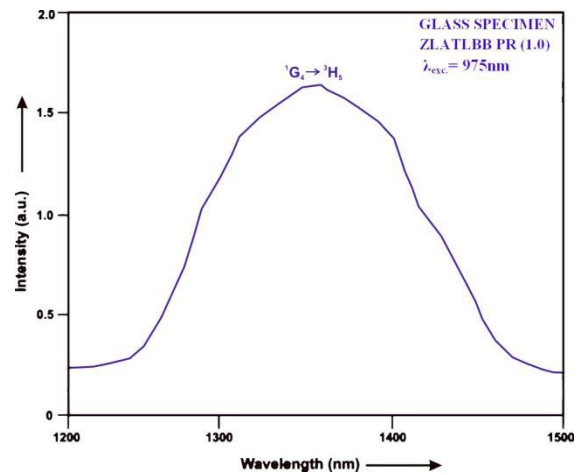
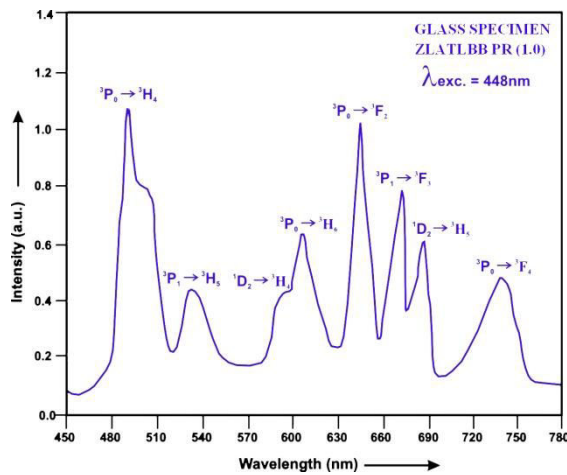


Fig.5: Excitation Spectrum of ZLATLBB PR (1.0) glass.

4.6. Fluorescence Spectrum

The fluorescence spectrum of Pr³⁺ doped in zinc lithium alumin tungsten lead bismuth borate glass is shown in Figure 6. There are nine broad bands (³P₀→³H₄), (³P₀→³H₅), (¹D₂→³H₄) (³P₀→³H₆), (³P₀→³F₂), (³P₁→³F₃), (¹D₂→³H₅), (³P₀→³F₄) and (¹G₄→³H₅) respectively for glass specimens.



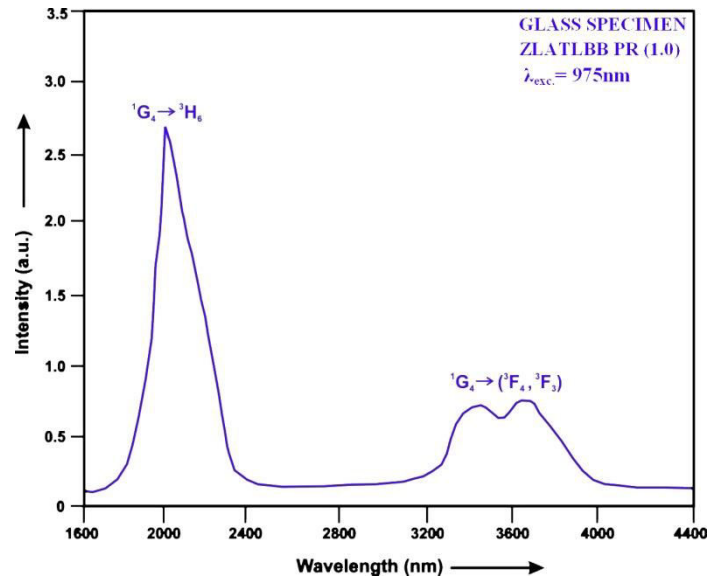


Fig.6: Fluorescence spectrum of ZLATLBB PR (1.0) glass.

Table6. Emission peak wave lengths (λ_p), radiative transition probability (A_{rad}), branching ratio (β_R), stimulated emission crosssection (σ_p), and radiative life time (τ) for various transitions in Pr^{3+} doped ZLATLBB glasses.

Transition	ZLATLBB PR (1.0)					ZLATLBB PR (1.5)				ZLATLBB PR (2.0)			
	λ_{em} (nm)	$A_{rad}(s^{-1})$	β	$\sigma_p (10^{21} cm^2)$	$\tau_r(\mu s)$	$A_{rad}(s^{-1})$	β	$\sigma_p(10^{21} cm^2)$	$\tau_r(\mu s)$	$A_{rad}(s^{-1})$	β	$\sigma_p (10^{21} cm^2)$	$\tau_r (10^{-4} cm^2)$
$^1P_1 \rightarrow ^3H_4$	485	1446.38	0.1240	0.456	85.762	751.49	0.0899	0.240	119.67	888.56	0.1383	0.299	155.65
$^1P_1 \rightarrow ^3H_5$	532	2548.67	0.2186	0.474		1634.89	0.1956	0.309		1626.02	0.2531	0.314	
$^1D_2 \rightarrow ^3H_4$	599	582.91	0.0499	0.217		453.23	0.0542	0.173		384.81	0.0598	0.152	
$^1P_1 \rightarrow ^3H_6$	602	500.34	0.0429	0.251		407.63	0.0488	0.212		336.03	0.0523	0.181	
$^3P_0 \rightarrow ^3F_4$	643	2307.49	0.1979	2.007		1913.54	0.2290	1.723		1026.00	0.1597	0.959	
$^3P_1 \rightarrow ^3F_3$	676	3542.28	0.3038	1.796		2693.65	0.3223	1.388		1708.64	0.2660	0.900	
$^1D_2 \rightarrow ^3H_4$	685	6.87	0.0006	0.0068		4.22	0.0005	0.0044		4.35	0.0007	0.005	
$^3P_0 \rightarrow ^3F_4$	730	267.18	0.0229	0.188		138.82	0.0166	0.1002		164.14	0.0255	0.122	
$^1G_4 \rightarrow ^3H_6$	1350	276.24	0.0237	0.881		218.47	0.0261	0.7023		181.53	0.0283	0.587	
$^1G_4 \rightarrow ^3H_5$	2025	160.65	0.0138	5.369		124.77	0.0149	4.244		94.13	0.0147	3.229	
$^1G_4 \rightarrow (^3F_4, ^3F_3)$	3555	21.09	0.0018	3.555	15.87	0.0019	2.719	10.43	0.0016	1.808			

V. CONCLUSION

In the present study, the glass samples of composition (35-x):Bi₂O₃:10ZnO:10Li₂O:10Al₂O₃:10WO₃:10PbO:15B₂O₃:xPr₂O₃ (where x =1, 1.5, 2 mol %) have been prepared by melt-quenching method. The large value of Balaji and Shankar parameters indicate that the prepared glass samples have good thermal stability. The stimulated emission cross-section (σ_p) has highest value for the transition ($^1G_4 \rightarrow ^3H_6$) in all the glass specimen doped with Pr^{3+} ion. This shows that ($^1G_4 \rightarrow ^3H_6$) transition is most probable transition and it useful for optoelectronic applications.

REFERENCES

- [1]. Meena, S.L. (2025). Spectral and Thermal and Raman Analysis of Ho³⁺ doped borophosphate glasses with large Balaji parameter, IOSR Appl.Phys.17,24-31.
- [2]. Sailaja, P., Mahamuda, Sk., Dedeepya, G., Alzahrani, J.S., Swapna, K., Venkateswarlu, M., Rao, A.S., Alrowaili, Z.A., Olorin oye, I.O., Al-Buriah, M.S. (2024). Effect of Eu³⁺ ions concentration on visible red luminescence and radiative shielding properties of SrO-Al₂O₃-BaCl₂-B₂O₃-TeO₂ glasses, Rad.Phys.Chem.216,111467.
- [3]. Dhinakaran, A.P., Vinothkumar, P., Senthil, T.S., Kalpana, S. (2024). Investigation on luminescent characteristics of Tb³⁺/Dy³⁺ co-doped borophosphate glass for cool white LED and radiation shielding applications, Appl.Phys.A,130,709
- [4]. Dogan, A., Erden, M., Esmer, K., Eryurek, G. (2021). Upconversion luminescence and temperature sensing characteristics of Ho³⁺/Yb³⁺ co-doped tellurite glasses, J.Non-Cryst.Solids,571,121055.
- [5]. Meena, S.L. (2024). Photoluminescence and Raman analysis of Nd³⁺ doped in yttrium zinc lithium sodium barium calcium aluminophosphate glasses, IOSR Appl.Phys.16,28-34.
- [6]. Lakshminarayana, G., Baki, S.O., Lira, A., Kityk, I.V., Caldino, U., Kaky, K.M., Mahdi, M.A. (2017). Structural, thermal and optical investigation of Dy³⁺ doped B₂O₃-WO₃-ZnO-Li₂O-Na₂O glasses for warm white light emitting applications, J.Lumin.186,283-300.
- [7]. Rani, P.R., Venkateswarlu, M., Mahamuda, S., Swapna, K., Deopa, N., Rao, A.S., Prakash, G.V. (2019). Structural, absorption and photoluminescence studies Sm³⁺ ions doped barium lead fluoroborate glasses for optoelectronic device applications. Mat. Research Bulletin,110, 159-168.
- [8]. Meena, S.L. (2017). Spectroscopic properties of Eu³⁺ doped in yttrium zinc lithium bismuth borate glasses, Int.J.Eng.Sci.6,30-36.
- [9]. Balakrishna, A., Rajesh, D. and Ratnakaram, Y.C. (2013). Structural and optical properties of Nd³⁺ in lithium fluoro-borate glass with relevant modifier oxides. Opt. Mater.,35, 2670–2676.
- [10]. Roopa, E.B. (2022). Impact of samarium ion concentration on the physical, structural and optical properties of multi-component borate glasses, J.Non-Cryst.Solids,596,121866
- [11]. Prabhu, N.S., Hegde, V., WaGH, A., Sayyed, M.I., Kamath, O.A. (2019). Physical, structure and optical properties of Sm³⁺ doped lithium zinc alimino borate glasses, J.Non-Cryst.Solids,515,116-124.
- [12]. Meena, S.L. (2025). Spectroscopic and photoluminescence properties of Ho³⁺ doped borate glasses with NIR light emission Applications, IOSR, Appl.Phys.17,34-40.
- [13]. ShivaKumar, B.N., Devaraja, C., Gedam, R.S., Eraiah, B., Jagadeesha Gowda, G.V., Harisha, G., Ashok Reddy, G.V. (2025). Implications of silver nitrate doping on the physical, structural and optical attributes of Na₂O-ZnO-borate glasses, J.Mol.Struct.1325,140985.
- [14]. Vijayasri, Rudramamba, K.S., Srikanth, T., Reddy, N.M., Nahha, M., Pratyusha, S. Reddy, M.R. (2023). Spectroscopic features of Tb³⁺ doped strontium zinc borate glasses for green laser applications, J.Mol.Struct.1274(3),134514
- [15]. Meena, S.L. (2020). Spectroscopic properties of Er³⁺ doped zinc lithium arsenic strontium vanadium bismuth borate glasses, IOSR Appl.Phys.12,05-10.
- [16]. Madhu, A., Eraiah, B., Manasa, P., Basavapoomima, Ch. (2018). Er³⁺ ions doped lithium-bismuth boro phosphate glass for 1532 nm emission and efficient red emission up conversion for telecommunication and lasing application, J.Non-Cryst.Solids,495,35-46.
- [17]. Meena, S.L. (2021). Spectral and Thermal and Raman Analysis of Tm³⁺ doped in phosphate glasses for optical temperature sensor applications, IOSR Appl.Phys.18,24-30.
- [18]. Meena, S.L. (2021). Spectral and Raman Analysis of Er³⁺ doped Zinc Lithium Antimony Sodalime Tellurite Glasses, Int.J.Eng.Sci.Inv.10,09-15.
- [19]. Judd, B.R. (1962). Optical Absorption Intensities of Rare Earth Ions. Physical Review, 127, 750.
- [20]. Ofelt, G.S. (1962). Intensities of Crystal Spectra of Rare Earth Ions. The J. Chem. Phys., 37, 511.
- [21]. Sinha, S.P. (1983). Systematics and properties of lanthanides, Reidel, Dordrecht.
- [22]. Krupke, W.F. (1974). IEEE J. Quantum Electron QE, 10,450.
- [23]. Meena, S.L. (2026). Spectral, Thermal and Luminescent properties of Nd³⁺ doped borophosphate glasses for 1075µm NIR Photonic broad band Amplification applications, glasses, IOSR Appl.Phys.18,16-23.
- [24]. Suthanthirakumar, P., Basavapoomima, Ch., Marimutha, K. (2017). Effect of Pr³⁺ ions concentration on the spectroscopic properties of zinc telluro-fluoroborate glasses for laser and optical amplifier, J.Lumin.187,392-402.
- [25]. Burtan, B., Cisowski, J., Mazurak, Z., Jarzabck, B., Czaja, M., Reben, M., Grelowska, I. (2014). Concentration dependent spectroscopic properties of Pr³⁺ ions in TeO₂-WO₃-PbO-La₂O₃ glass, J.Non-Cryst.Solids 400,21-26.



INTERNATIONAL
STANDARD
SERIAL
NUMBER
INDIA



INTERNATIONAL JOURNAL OF INNOVATIVE RESEARCH

IN SCIENCE | ENGINEERING | TECHNOLOGY

 9940 572 462  6381 907 438  ijirset@gmail.com



www.ijirset.com

Scan to save the contact details